JMEPEG (2013) 22:94–103
DOI: 10.1007/s11665-012-0231-2

1059-9495/$19.00

Tribological Analysis of Copper-Coated Graphite Particle-Reinforced A359 Al/5 wt.% SiC Composites

C.B. Lin, T.C. Wang, Z.C. Chang, and H.Y. Chu

(Submitted September 5, 2010; in revised form September 24, 2011; published online May 9, 2012)

Copper-coated graphite particles can be mass-produced by the cementation process using simple equipment. Graphite particulates that were coated with electroless copper and 5 wt.% SiC particulates were introduced into an aluminum alloy by compocasting to make A359 Al/5 wt.% SiC(p) composite that contained 2, 4, 6, and 8 wt.% graphite particulate composite. The effects of SiC particles, quantity of graphite particles, normal loading, sliding speed and wear debris on the coefficient of friction, and the wear rate were investigated. The results thus obtained indicate that the wear properties were improved by adding small amounts of SiC and graphite particles into the A359 Al alloy. The coefficient of friction of the A359 Al/5 wt.% SiC(p) composite that contained 6.0 wt.% graphite particulates was reduced to 0.246 and the amount of graphite film that was released on the worn surface increased with the graphite particulate content. The coefficient of friction and the wear rate were insensitive to the variation in the sliding speed and normal loading.

Keywords aluminum matrix composites, graphite, silicon carbide, wear

1. Introduction

Aluminum alloy is extensively used as a matrix material because of its high specific strength, high thermal conductivity, and low density. However, it has poor anti-wear characteristics and it cannot resist the severe wear that occurs between a liner and piston rings, reducing engine efficiency. Some methods for solving this problem have been proposed. One involves incorporating solid lubricant particles or flakes such as graphite, MoS_2, or CaF_2 into the aluminum alloy matrix (Ref 1, 2). Another involves adding Pb to the Al alloys (Ref 3-5). According to Srivastava et al. (Ref 3), the wear resistance of Al-Si alloy increases with Pb content and the alloy that contains 20% Pb has a reduced coefficient of friction. A number of aluminum matrix composites have been developed for potential tribological applications in cylinder liners because of their ability to resist seizure and scuffing under adverse engine running conditions. According to Gibson et al. (Ref 2), adding 2.0 wt.% graphite particles to aluminum alloy reduces the friction coefficient, wear rate, and contact temperature of the composite, and adding 8.0 wt.% graphite particles makes the composite brittle and increases the wear rate. Biswas and Bai (Ref 6) showed that the wear rate of the graphite particle-reinforced aluminum increases with the amount particles.

Graphite is the most common solid lubricant since it is inexpensive and very effective. However, the bonding strength between graphite and the Al matrix is very poor, because the contact angle between graphite and aluminum is very low (Ref 7). When an externally applied stress is exerted on an aluminum matrix/graphite particles composite, several cracks or voids can be found at the interface between the matrix and the graphite particles, reducing its bulk strength. Rohatgi and Prasad (Ref 8) obtained the same results and demonstrated that they follow from the low strength at the interface between the graphite and the aluminum alloy. To improve the wettability and the bonding strength between aluminum and graphite particles, the surfaces of the graphite particles are coated with a layer of copper, nickel, or magnesium as a wetting metal (Ref 9-11). According to Jha et al. (Ref 1), the porosity encountered in the process of fabrication of aluminum matrix/graphite particle composite embrittles the material with crack nucleation and reduction in fracture toughness and elongation of the composites leading to increased wear rate. According to Funatni et al. (Ref 12), an engine system loses approximately 41% of its energy output because of wearing out of its parts. An engine cylinder that is made from an Al alloy/graphite particulate composite has a higher seizure resistance, a lower frictional coefficient, and a lower wear rate than one made from an aluminum matrix that is reinforced with silicon carbide particulates.

Several methods of fabricating aluminum matrix/graphite particle composites have been studied and proposed. These include *the compocasting method* (Ref 13), *the vortex method* (Ref 14), *squeeze casting* (Ref 15), *powder metallurgy* (Ref 16), *vacuum infiltration* (Ref 17), *mechanical milling* (Ref 18), *melt-conditioned high-pressure die casting (MC-HPDC)* (Ref 19), and others. Composites that are fabricated using the powder metallurgy method have a higher wear rate than those fabricated using compocasting, vortex, squeeze casting, and

C.B. Lin and **T.C. Wang**, Department of Mechanical and Electro-Mechanical Engineering, Tamkang University, Tamsui, New Taipei, Taiwan, ROC; **Z.C. Chang**, Department of Mechanical Engineering, National Chin-Yi University of Technology, Taiping City, Taichung County, Taiwan, ROC; and **H.Y. Chu**, Department of Mechanical Engineering, Kung-Shan University of Technology, Tainan City, Taiwan, ROC. Contact e-mail: cblin@mail.tku.edu.tw.

squeeze infiltration methods. The fabrication method appears to affect the tribological performance of the aluminum alloy/graphite particle composites. The compocasting method was utilized herein. According to Suresh and Sridhara (Ref 20), aluminum alloy matrix composites reinforced with silicon carbide (SiC) and graphite (Gr.) are extensively used due to high strength and wear resistance.

Therefore, this work proposes a simple piece of equipment for mass-fabricating copper-coated graphite particles and utilizes the compocasting method to make A359 Al/5 wt.% SiC + 2, 4, 6, 8 wt.% graphite particulate composites. The effect of the amount of graphite particles, sliding speed, and normal loading on the tribological properties are also studied using dry wear tests. Finally, the experimental data were analyzed and discussed.

2. Experimental Details

2.1 Materials and Processing

The contact angle of aluminum with graphite is about 155 °C and is reported to remain unwettable at temperatures between the melting point of aluminum and 1080 °C (Ref 8). Poor wettability causes inadequate interface bonding between the aluminum matrix and the graphite particulate. Additionally, adding a graphite particulate directly into molten aluminum is difficult. In the experiment in this work, to improve the surface wettability and strength of the interface bonding between aluminum alloy and graphite particulate, the surfaces of the graphite particles are coated with electroless copper by a cementation process, in which the chemical reaction is $CuSO_{4\ (aq)} + Zn_{(s)} \rightarrow ZnSO_{4\ (aq)} + Cu_{(s)}$. The copper ions are replaced by zinc via heterogeneous secondary nucleation process. Before the electroless coating of copper, the graphite particles are cleaned using acetone to prevent contamination by impurities. Glacial acetic acid is added to the cupric sulfate solution as a wetting agent. Figure 1(a) presents the simple device for mass-fabricating an electroless copper coating. The copper coating of graphite particles proceeds as follows:

1. The graphite particles are immersed in acetone solution, which is then twice oscillated in an ultrasonic oscillating container. The duration of each oscillation is around 20 min. The solution is then dried in air at 200 °C.
2. 0.3 M cupric sulfate solution is made from mixing $CuSO_4 \cdot 5H_2O$ with the appropriate amount of distilled water. 0.1 wt.% glacial acetic acid is added and mixed uniformly. This solution serves as the electrolyte.
3. Copper coating process: The graphite particles are added to the agitator after the electrolyte is poured. The particles are uniformly distributed in the electrolyte using the agitation system, which is driven by motor as shown in Fig. 2. Zinc pellets are put in a net and immersed in the electrolyte. During agitation, the graphite particles are taken out periodically to be observed under a JEOL-JSM-5400 scanning electronic microscope (SEM) and the cementation process is deemed to be complete when the copper coating layer is distributed uniformly on the surfaces of the graphite particulates.
4. The copper-coated graphite particles are placed in a strainer. De-ionized water is used to flush the SO_4^{2-} and Zn^{2+} ions away. The copper-coated graphite particles are then placed in a vacuum furnace to dry and degas them. The dried copper-coated graphite particles are then screened to prevent aggregation.

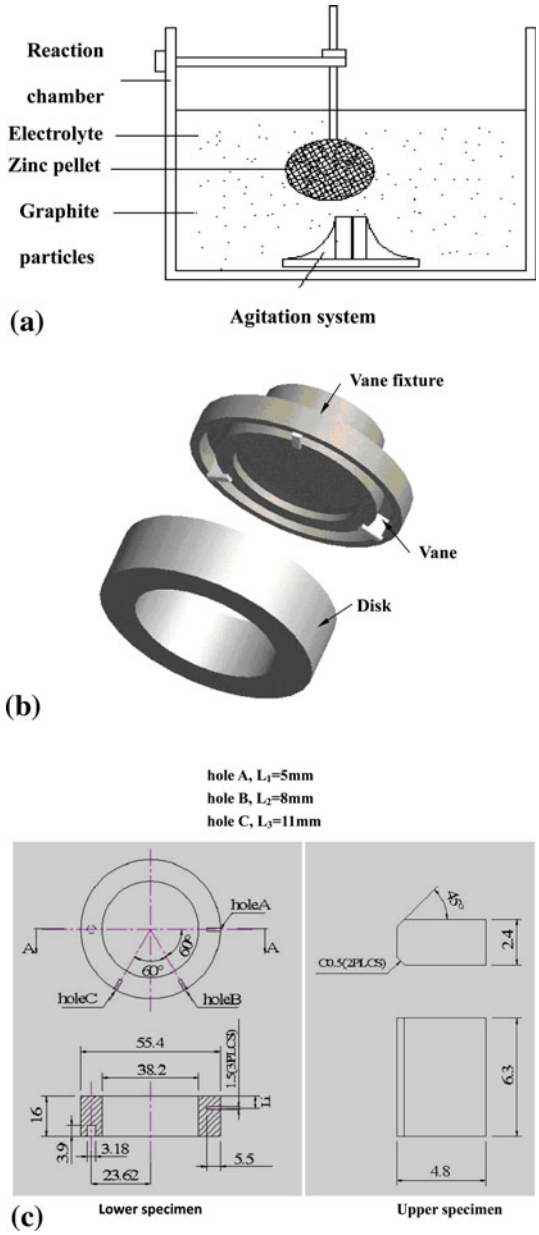

Fig. 1 (a) Fabrication of copper-coated graphite particles, (b) vanes-on-disk wear test, and (c) dimensions of vane and ring-type disk

Following the above process, the dried copper-coated graphite particles are placed in sealed container. The morphology of the copper-coated graphite particles is observed using a JEOL-JSM-5400 SEM.

A359 Al alloy (9.50%Si-0.12%Fe-0.10%Cu-0.1%Mn-0.70%Mg-0.10%Zn-0.20%Ti) is used as matrix in the experiment. Silicon carbide (SiC) and graphite particulates are selected as the reinforced phase and the lubricant phase, respectively. A359 Al/5 wt.% SiC composites that include copper-coated graphite particles are fabricated by the following compocasting process. (1) A359 aluminum alloy is placed in a

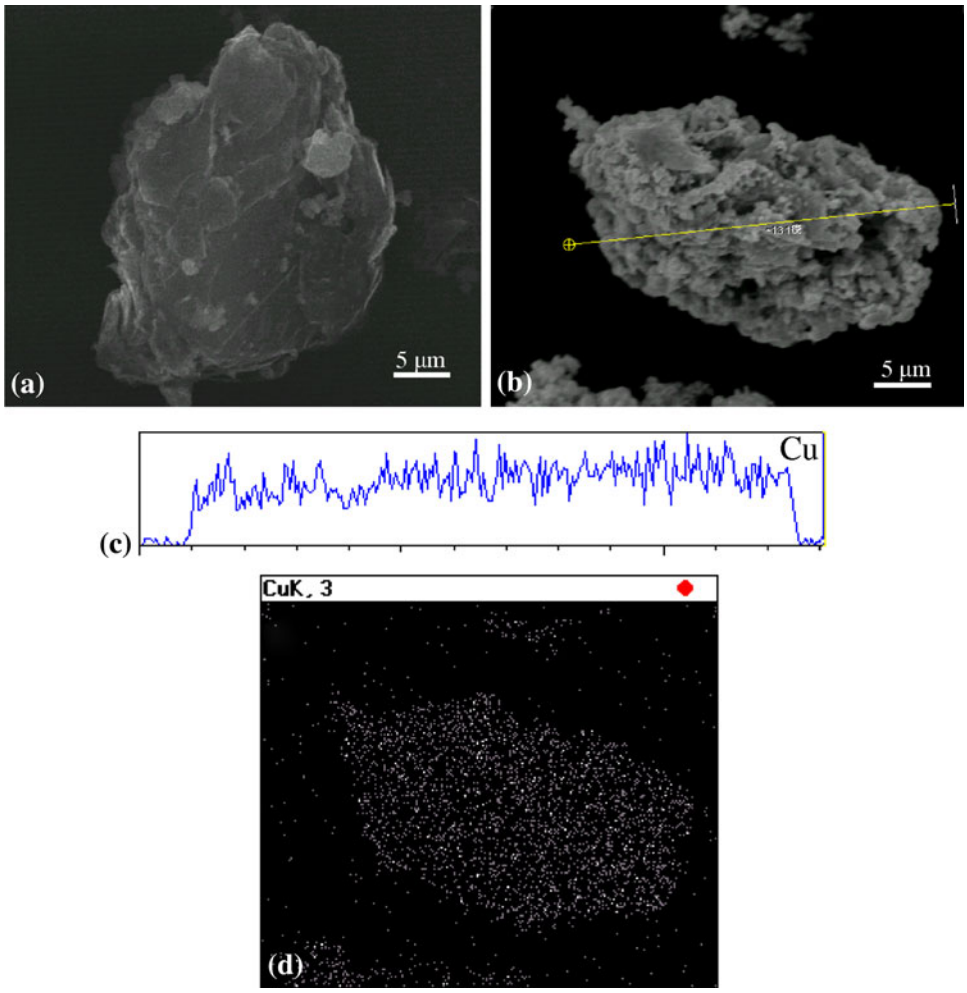

Fig. 2 (a) and (b) SEM photographs of graphite particle before and after coating with copper; Cu element is detected by (c) EDS and (d) mapping of copper-coated graphite surface

graphite crucible and heated to 700 °C until it is completely melted; the crucible is then degassed; (2) 5 wt.% silicon carbide particles are added to the molten A359 Al that incorporates irregularly shaped, γ-phase SiC particles with an average size of 15 μm (Ref 21); (3) the composite semi-solid slurry is mixed in the temperature range between the liquidus and the solidus temperatures. Then 2, 4, 6, or 8 wt.% irregularly shaped copper-coated graphite particles with an average size of 20 μm are introduced into the semi-solid slurry. The graphite particles are entrapped effectively by the primary solid crystal of the semi-solid slurry. The proportion of solid is around 43%. A stainless steel stirring rod is used to disperse these particles (SiC and Gr.) uniformly in the matrix. It is plasma-coated with a ZrO_2 layer to prevent it from being corroded by heating, and driven by a reciprocating motor. The main purpose of the reciprocating agitation is to create more vortexes in the molten aluminum to increase the uniformity of the distribution of the SiC particles and copper-coated graphite particles; (4) after a fixed amount of graphite particulates has been added, the composites in the slurry state are squeezed into a permanent mold that is preheated at 550 °C under 200 T pressure; (5) the composites are subsequently homogenized at 380 °C in air for 4 h to reduce solidification-induced segregation.

The distribution of particles in the aluminum alloy matrix is observed using a Nikon OPTIPHOT-100 optical microscope (OM). Before the observations are made, the composites must be ground using 2000 grit size SiC abrasive paper, and then polished using a 0.3 μm Al_2O_3 suspension.

2.2 Hardness Testing

Hardness testing was carried out using a B-scale Rockwell hardness tester under a load of 100 kgf and period of 30 s. To establish reproducibility of results, at least six tests were performed. Before the wear test, each specimen was ground using 1 μm alumina suspension liquid, while ensuring that the wear surface of the specimen was in complete contact with the surface of the disk. The vanes were ground to a roughness of Ra = 0.2 μm, and the disks to Ra = 0.15 μm.

2.3 Wear Testing

Vanes-on-disk wear testing was performed to evaluate the tribological performance of A359 Al that was blended with 5 wt.% SiC and 2, 4, 6, or 8 wt.% graphite particles. Figure 1(b) schematically depicts the vanes-on-a-disk wear test. Three vanes serve as the upper specimens of the vanes-on-disk. The vanes are plugged into the vane fixture. The disk (lower specimen) is made of A332.2 aluminum alloy (11.5%Si-0.90%Fe-1.15%Cu-0.10%Mn-1.10%Mg-2.50%Ni-0.01%Zn-0.20%Ti), which is extensively used in engine cylinder sleeves in the automotive

industry. Figure 1(c) presents the dimensions of the vane and the ring-type disks. T6 heat treatment is applied to both the upper and the lower specimens after machining of the workpieces have been machined to remove residual stresses and increase hardness and mechanical strength. To apply the T6 heat treatment, the vane specimens are solutionized at 540 ± 3 °C for 8 h, and subsequently quenched in water (27 ± 3 °C); they are then aged at 155 ± 3 °C for 4 h before being cooled in air to 25 ± 3 °C; the disks are solutionized at 530 ± 3 °C for 1.5 h, and subsequently quenched in water (27 ± 3 °C); they are then aged at 175 ± 3 °C for 8 h before being cooled in air to 25 ± 3 °C.

The vanes-on-disk wear test was performed on a Falex-6 wear test machine. Reciprocating motion was used because it is similar to the motion of the piston ring in an engine. Wear tests were performed at 25 °C (room temperature) and dry conditions under applied loads of 0.37, 0.49, and 0.62 MPa., and sliding speeds of 0.55, 0.73, and 0.92 m/s. A fixed sliding distance of 60 m was used in all tests, and under each test condition, at least three runs were performed. Before and after the wear test, the samples were ultrasonically cleaned in acetone, dried, and then weighed using an electronic balance with a resolution of 0.1 mg. Wear loses were obtained by determining the weight loss of the specimens during the tests. The wear rate was calculated by converting the measured weight loss (±0.1 mg) to a volume loss using the apparent density, which was measured by Archimedes method:

$$W\ (\mathrm{mm}^3/\mathrm{m}) = \frac{\text{mass loss (g)/apparent density } (\mathrm{g}/\mathrm{mm}^3)}{\text{sliding distance (m)}}.$$

To evaluate the tribological performance of the A359 aluminum matrix and the composites, the worn surfaces, cross-sections below the worn surfaces, and wear debris particles were investigated by LEO-5210 SEM. The specimens were coated with gold for 2 min before they were examined, and the wear mechanism was probed using an electrical contact resistance (ECR) device. The friction coefficient, f, was obtained using the equation $f = T/Lr$, where T is the induced friction torque, L is the normal load, and r is the mean contact radius of the rotating vanes. The worn surface roughness of the composites was evaluated by measuring surface texture using a stylus-type instrument. The worn surface profiles were recorded across the wear tracks. The surface roughness Ra (μm) was used to detect the worn surface roughness after the wear tests.

3. Results and Discussion

Figure 2(a) and (b) shows SEM micrographs of graphite particulates before and after coating with copper, respectively. Figure 2(c) and (d) presents the line-profile and mapping of the graphite particulates after coating. The copper coating layer is distributed uniformly on the surface of the particulate graphite. This work proposes a simple apparatus to eliminate the shortcomings of a previously presented process (Ref 22) and reduces the cementation time in two ways. (1) A zinc plate is used instead of zinc pellets, increasing the probability of impact between copper ions and graphite particles, and (2) the electrolyte is passed continuously through the open channel through the packed-zinc pellets by agitation flow, increasing the cementation rate.

Figure 3 displays the OM micrographs of A359 aluminum alloy, A359 Al/5 wt.% SiC composite, and the composites with 2, 4, 6, or 8 wt.% graphite particles. Needle-like eutectic Si appeared on the A359 aluminum alloy matrix and SiC particles segregated in the inter-dendritic regions, as shown in Fig. 3(a) and (b). The surfaces of the graphite particles were coated with layers of copper, which improved the wettability between aluminum and the particles, as shown in Fig. 3(e). Extensive clustering of graphite and porosity was observed when the graphite content was large, as shown in Fig. 3(f) and (g).

3.1 Hardness

Figure 4 presents the hardness of A359 aluminum alloy, A332.2 aluminum alloy, A359 Al/5 wt.% SiC composite, and the composites that contained 2, 4, 6, or 8 wt.% graphite particles. The hardness of A359 aluminum alloy/5 wt.% SiC composite only slightly exceeded that of A359 aluminum alloy, because the SiC particles were not dispersed uniformly throughout the A359 aluminum alloy matrix, as seen in the optical micrograph in Fig. 3(b).The lower specimen (disk specimen) that was made from A332.2 aluminum alloy was harder than the upper specimen (ring specimen) that was made from A359 Al/5 wt.% SiC composite that contained 2, 4, 6, or 8 wt.% graphite particles. The hardness decreased linearly as the graphite particle content increased because the hardness of the laminated-graphite was much lower than that of the A359 aluminum alloy.

3.2 Friction Coefficient and Wear Rate

Figure 5(a)-(c) plots the variations in the friction coefficient and the wear rate of the A359 aluminum alloy and the composites at normal loads of 0.37, 0.49, and 0.62 MPa and sliding speeds of 0.55, 0.73, or 0.92 m/s. At normal loads of 0.37, 0.49, and 0.62 MPa, the A359 aluminum alloy had the highest friction coefficient and the A359 Al/5 wt.% SiC composite that contained 6 wt.% graphite particles had the lowest. However, as the graphite content increased to 8 wt.%, the friction coefficient no longer decreased but increased. Figure 6(a)-(f) presents the worn surface morphologies of A359 aluminum alloy, A359 Al/5 wt.% SiC composite, and the composites that contained 2, 4, 6, or 8 wt.% graphite particles under the highest load of 0.62 MPa and the highest sliding speed of 0.92 m/s. Figure 6(a), which presents the worn surface morphology of the A359 aluminum alloy, clearly reveals that severe adhesive wear is the dominant wear mechanism and the worn surface is very rough (Ra = 9.7 μm). The adhesive wear of the A359 Al/5 wt.% SiC composite is less than that of the A359 aluminum alloy, as shown in Fig. 6(b), because the SiC particulates lessened the severity of grooving, presumably by increasing the hardness of the material. Figure 6(c) presents the rough worn surface morphology of the A359 Al/5 wt.% SiC + 2 wt.% Gr. composite (Ra = 7.4 μm), which contains less graphite than the other graphite-containing composites and the lower hardness of the Al/5 wt.% SiC + 2 wt.% Gr.(p) composite than that of the A359 aluminum alloy thus cannot effectively prevent ploughing on the sliding surface of the composites, and decrease the friction coefficient. From Fig. 6(d) and (e), the worn surface of the A359 Al/5 wt.% SiC composite that contained 4 or 6 wt.% graphite particles was covered more uniformly the lubricating film, preventing direct contact between the upper and the lower specimens, reducing the transfer of shear stress to the sliding surface, and thus reducing the friction coefficient. The composites, regardless of their graphite particle content, exhibit no graphite

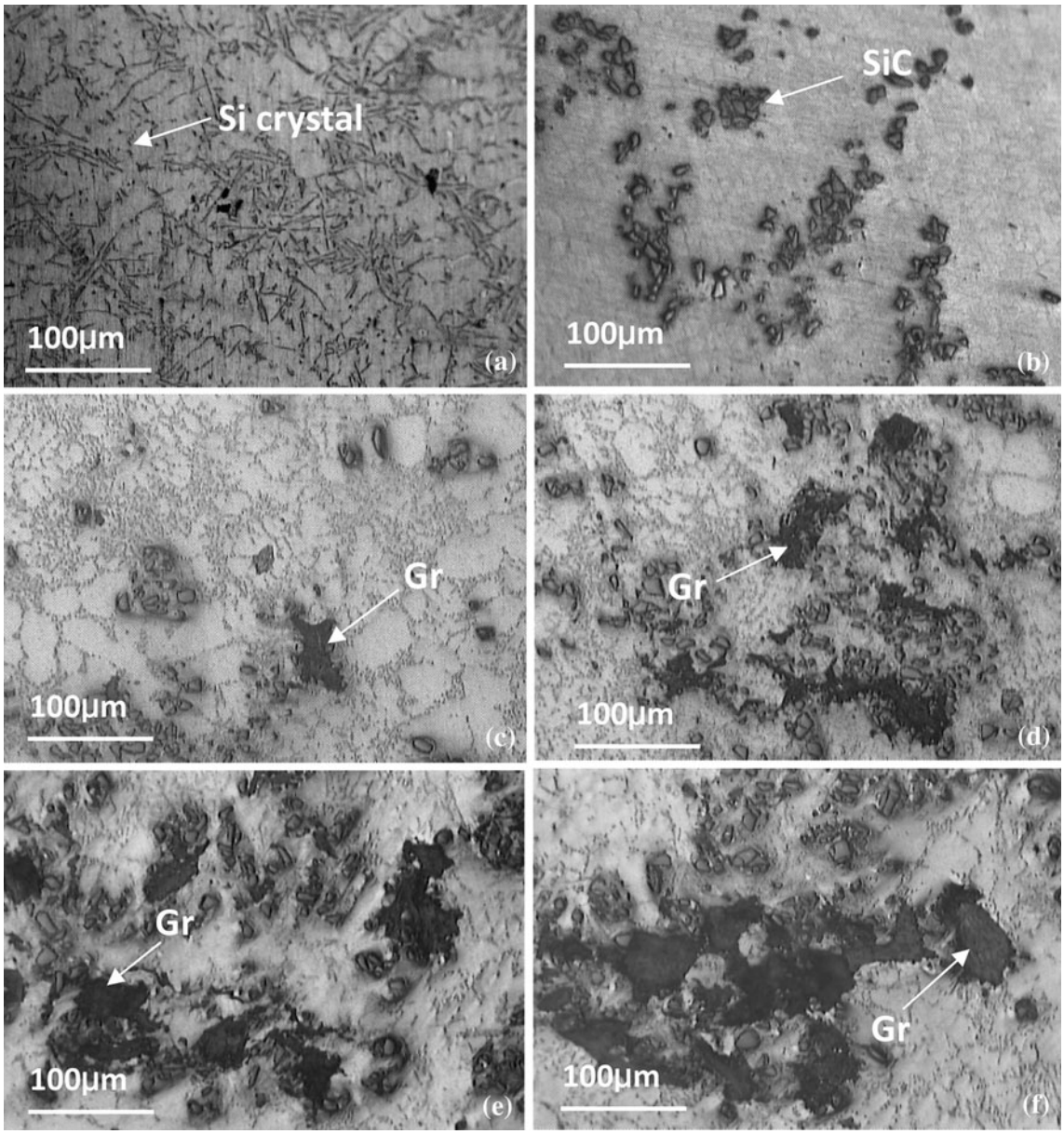

Fig. 3 Microstructures of (a) A359 aluminum; (b) A359 Al/SiC composite; and composites that contain (c) 2 wt.%, (d) 4 wt.%, (e) 6 wt.%, and (f) 8 wt.% graphite particles; (g) extensive clustering of the graphite content 8 wt.% graphite particles

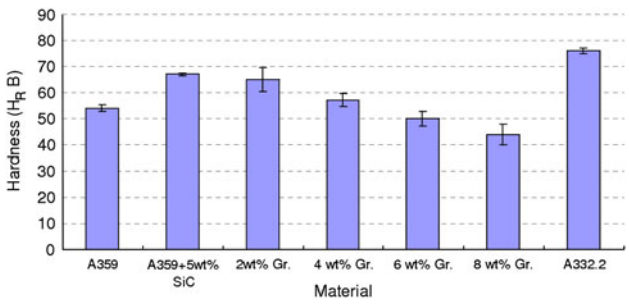

Fig. 4 Hardness of A359 aluminum alloy, A332.2 aluminum alloy, A359 Al/5 wt.% SiC composite, and composites that contain 2, 4, 6, or 8 wt.% graphite particles

agglomeration and the copper coating exhibits very good bonding strength between the graphite particle and the A359 aluminum alloy. The roughness of the worn surface at graphite contents of 4 and 6 wt.% is Ra = 2.84 μm and Ra = 2.10 μm, because the graphite particles are released and cover the mutually sliding surfaces, forming a lubricating film. Importantly, the worn surface exhibits no obvious cavity. Even if the Al/5 wt.% SiC + 8 wt.% Gr.(p) composite can form a graphite lubricant film on the worn surface, the high graphite particulate content causes easy clustering of graphite, promoting crack nucleation within the particulate, and causing brittle fracture in the region of clustering. Cavities form on the worn surface, as shown in Fig. 6(f), increasing the coefficient of friction. However, from the SEM photographs of the surface of the lower ring-type A332.2 Al alloy disk, shown in Fig. 7, the

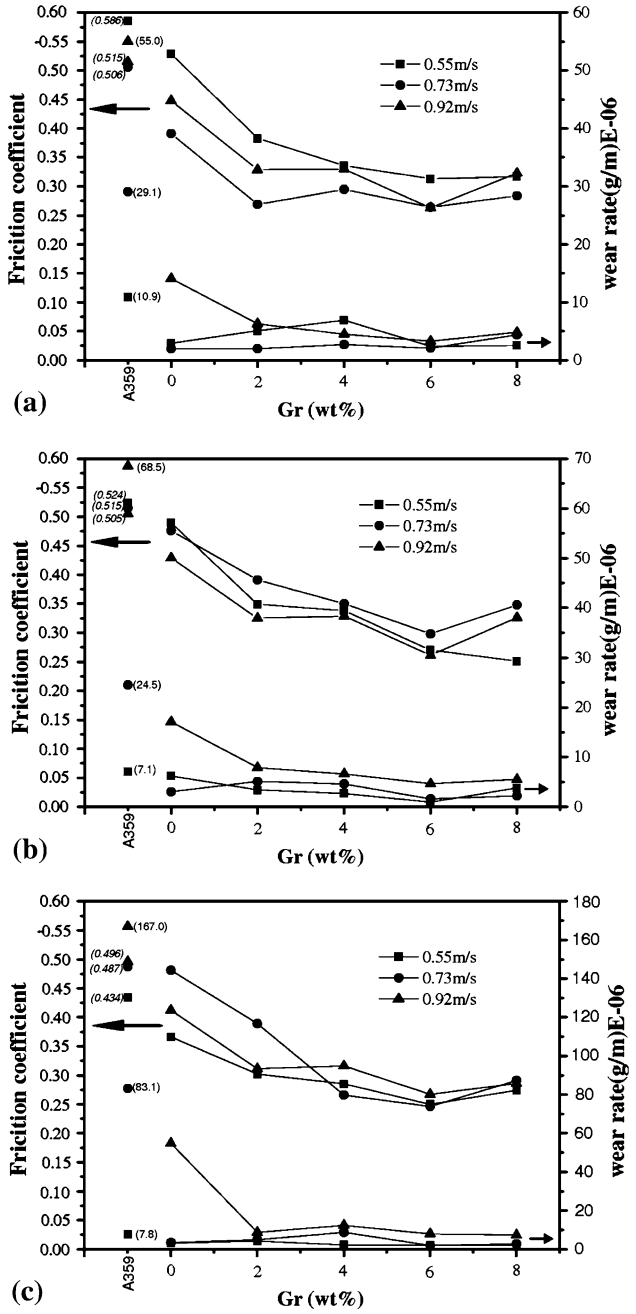

Fig. 5 Friction coefficient and wear rate of A359 aluminum alloy, A359 Al/5 wt.% SiC composite, and composite that contains 2, 4, 6, or 8 wt.% graphite particles under normal load of (a) 0.37 MPa, (b) 0.49 MPa, and (c) 0.62 MPa

worn surface becomes smoother as the Gr. content increases from 2 to 6 wt.% (Ra = 5.6 μm to Ra = 1.7 μm).

According to Fig. 5, the sliding speed has less of an effect on the friction coefficient of the materials, especially the A359 Al/5 wt.% SiC composites that contain 2-8 wt.% graphite particles, because all of the graphite lubricant film is formed between the worn surfaces, regardless of the sliding speed, and the particulate graphite can reduce plastic deformation on the worn surface.

Additionally, the normal load has less influence on the friction coefficient because of the reciprocal effect of shear stress and the graphite lubricant film.

The wear rates of the materials, based on their graphite content, descend in the order $W_{A359Al} > W_{A359Al/5\ wt.\%SiC(p)} > W_{A359Al/5\ wt.\%SiC(p)+2\ wt.\%Gr.(p)} > W_{A359Al/5\ wt.\%SiC(p)+4\ wt.\%Gr.(p)} \approx W_{A359Al/5\ wt.\%SiC(p)+8\ wt.\%Gr.(p)} > W_{A359Al/5\ wt.\%SiC(p)+6\ wt.\%Gr.(p)}$, as shown in Fig. 5. The soft matrix of the A359 aluminum alloy undergoes plastic deformation, forming several ploughs and resulting in a high wear rate, increasing the severity of scuffing. The presence of the silicon carbide reinforcement in the A359 aluminum alloy contributes towards increased resistance to seizure. The A359 Al/5 wt.% SiC composite with 2-6 wt.% graphite particles forms a graphite lubricating film, which lowers the wear rate, because most surfaces are covered with this film, reducing the shear forces that are transmitted from them to the sub-surface region. The amount of lubricating graphite film increases with the graphite content and the film is squeezed onto the sliding surface, which it easily covers the surface of the aluminum matrix. The A359 Al/5 wt.% SiC composite that contains 8 wt.% graphite particles exhibits several brittle fractures in the worn surface, resulting in a higher wear rate than that of the Al/6 wt.% Gr.(p) composite. Figure 8 presents the cross-sectional morphology of the A359 Al/5 wt.% SiC composite and the A359 Al/5 wt.% SiC composite that contains 6 wt.% graphite particles. The presence of the silicon carbides reinforcement in the A359 aluminum alloy of the A359 Al/5 wt.% SiC composite increases its resistance to seizure as shown in Fig. 8(a). Additionally, the silicon particles increase the hardness of the A356 alloy at its sliding wear surface that is in contact with the A332.2 aluminum alloy, providing resistance against shear deformation. When 6 wt.% graphite particles are added to the matrix, richer graphite lubricating films the dark layer on the surface of the specimen. The thickness of the graphite film is approximately the extruded height of the SiC particles, and the films that are "squeezed out" of the graphite particulates are elongated in the direction of the shear, as shown in Fig. 8(b). However, the A359 Al/5 wt.% SiC composite that contains 6 wt.% graphite particulates had a lower wear rate than the other specimens that contained different amounts of particulate graphite. This optimal amount of particulate graphite is squeezed onto the sliding surface of the aluminum matrix, easily covering it. Clearly, optimal values of graphite content produce a very effective lubricating film that protects against severe wear. The wear rate of the aluminum matrix and the composites was insensitive to the variation in sliding speed and normal loading. The formation of a lubricating graphite film on the tribosurface is considered to be the primary cause of the low friction and wear of composites.

3.3 Wear Debris and Electrical Contact Resistance

Figure 9(a)-(f) presents the wear debris of the A359 aluminum alloy, A359 Al/5 wt.% SiC composite and the composites that contain 2, 4, 6, or 8 wt.% graphite particles at a normal load of 0.62 MPa and a sliding speed of 0.92 m/s. The particles of wear debris of the aluminum alloy without added graphite is quite large and long, because of the severity of ploughing and microcutting. The severity of wear decreases as the graphite content in the composites increases, since the debris becomes smaller as the graphite particle content increases. However, the composites that contain 8 wt.% graphite particles exhibit several brittle fractures, which are observed on the worn surface. Accordingly, a comparison between Fig. 9(e) and (f) reveals that 8 wt.% graphite contain

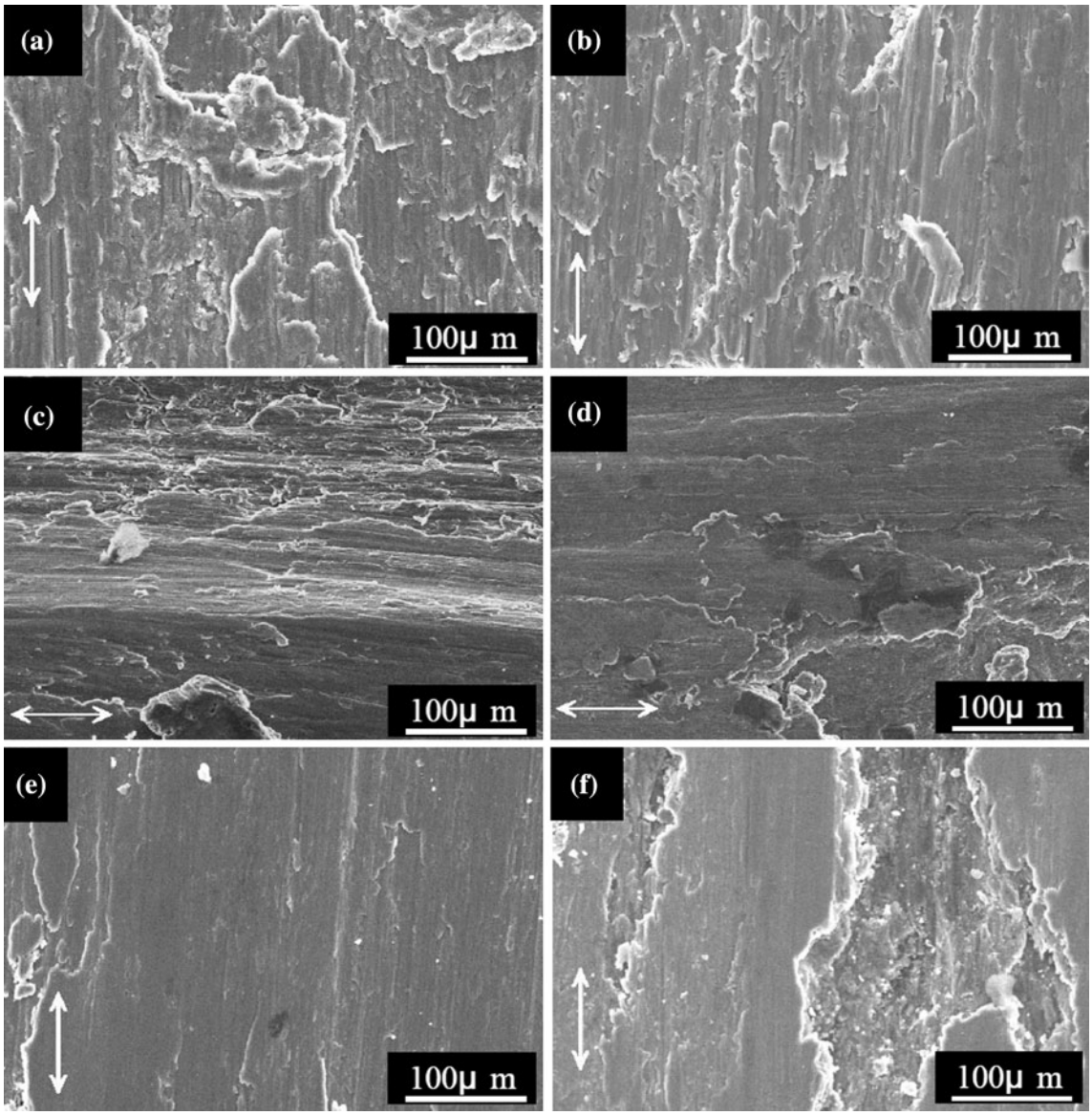

Fig. 6 Worn surface morphologies of (a) A359 aluminum, (b) A359 Al/SiC composite, and composite that contains (c) 2 wt.%, (d) 4 wt.%, (e) 6 wt.%, and (f) 8 wt.% graphite particles at heaviest load of 0.62 MPa and highest sliding speed of 0.92 m/s

yields some larger pieces of debris than obtained using other composites.

The ECR that is established under dry contacts can be measured to estimate the contact phenomenon: a lower ECR suggests a larger contact area. The ECR of the A359 Al is larger than that of other materials because of its relatively large and long pieces of wear debris, as shown in Fig. 10(a). The ECR declines as the amount of particulate graphite in the A359 Al/5 wt.% SiC composite increases between 2 and 6 wt.%. Since Al/2 wt.% Gr.(p) composite yields the largest wear debris, third-body wear may occur and the wear debris that Si entrapped between the two surfaces may have undergone a sliding motion rather than a rolling motion. As the graphite content increases to 6 wt.%, the pieces of wear debris become smaller; therefore, the probability of direct contact between the two surfaces increases. However, the A359 Al/5 wt.% SiC composite that contains 6 wt.% graphite particulates had a relatively lower ECR, as shown in Fig. 10. A comparison of Fig. 9(e) and (f) reveals some larger wear debris from the material with 8 wt.% graphite particles, and a slightly larger contact area than in the case of the 6 wt.% graphite particle content.

These results indicate that the wear particles, their size, and their types of motion strong affect ECR: larger debris corresponds to a higher ECR. The sliding speed has less effect than these factors on ECR As the sliding speed increases, the contact resistance varies only slightly, perhaps because plastic deformations that occur at the three sliding speeds considered herein at fixed normal loading do not differ significantly, and so the contact areas and wear debris are also of the same order or magnitude.

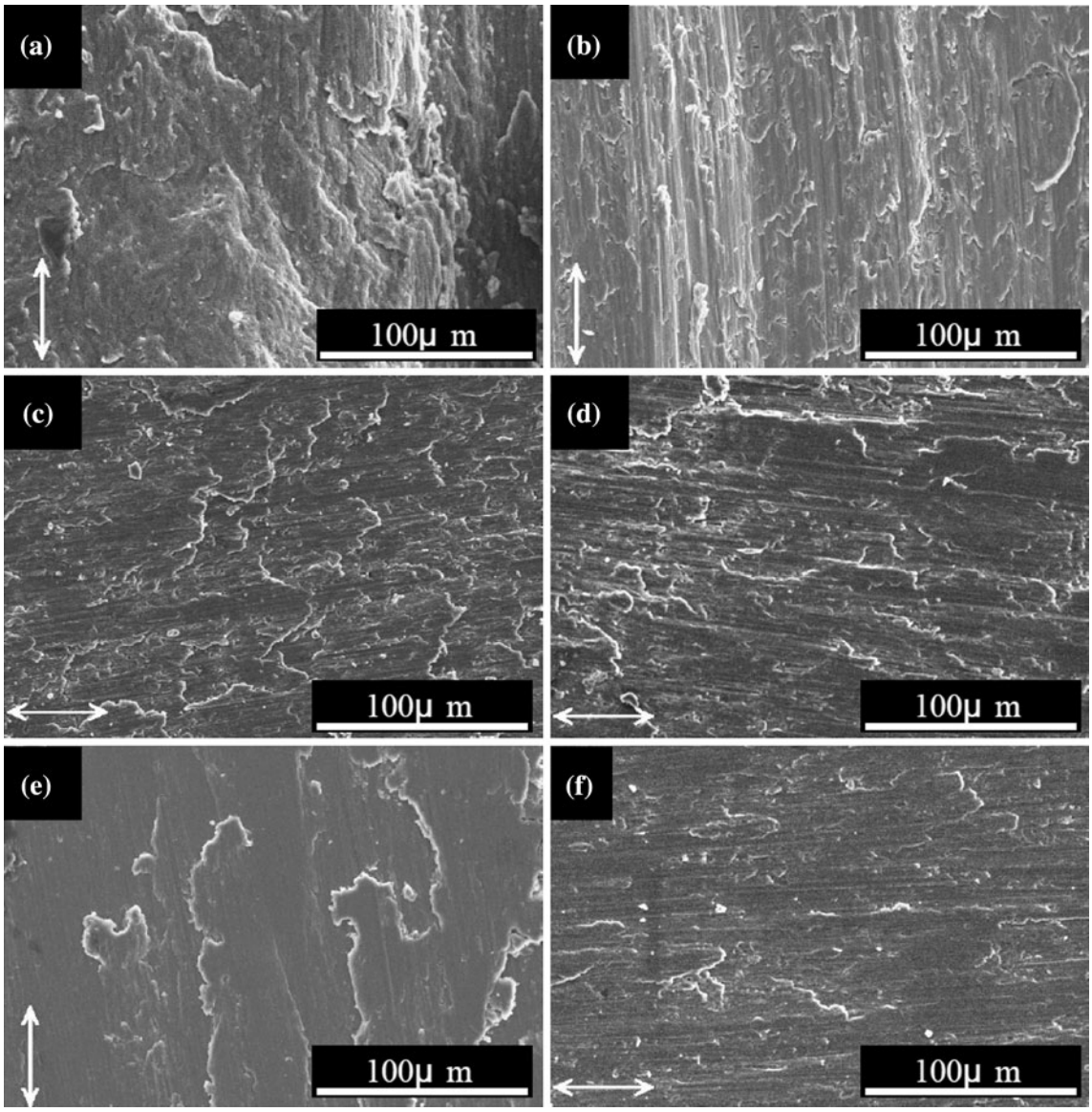

Fig. 7 Worn surface of A332.2 aluminum alloy with (a) A359 aluminum, (b) A359 Al/SiC composite, and composite that contains (c) 2 wt.%, (d) 4 wt.%, (e) 6 wt.% and (f) 8 wt.% graphite particles

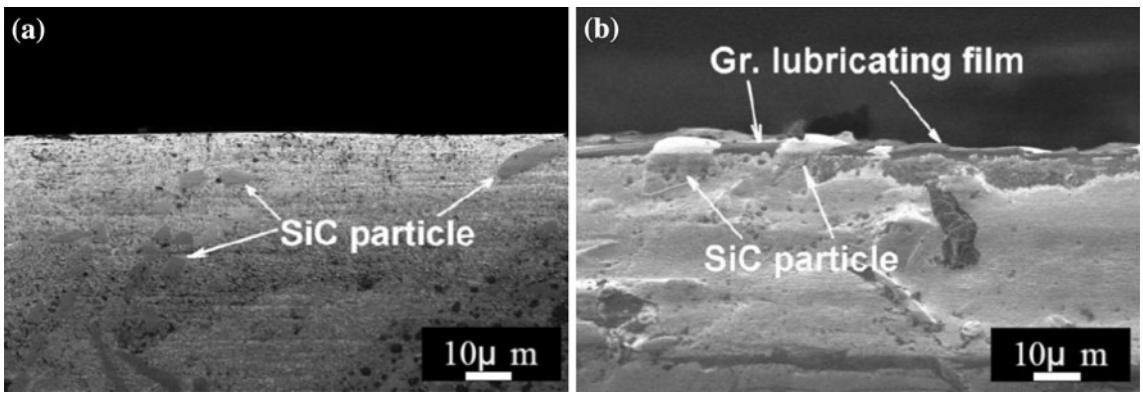

Fig. 8 Cross-sectional morphology of (a) A359 Al/5 wt.% SiC composite and (b) A359 Al/5 wt.% SiC composite that contains 6 wt.% graphite particles

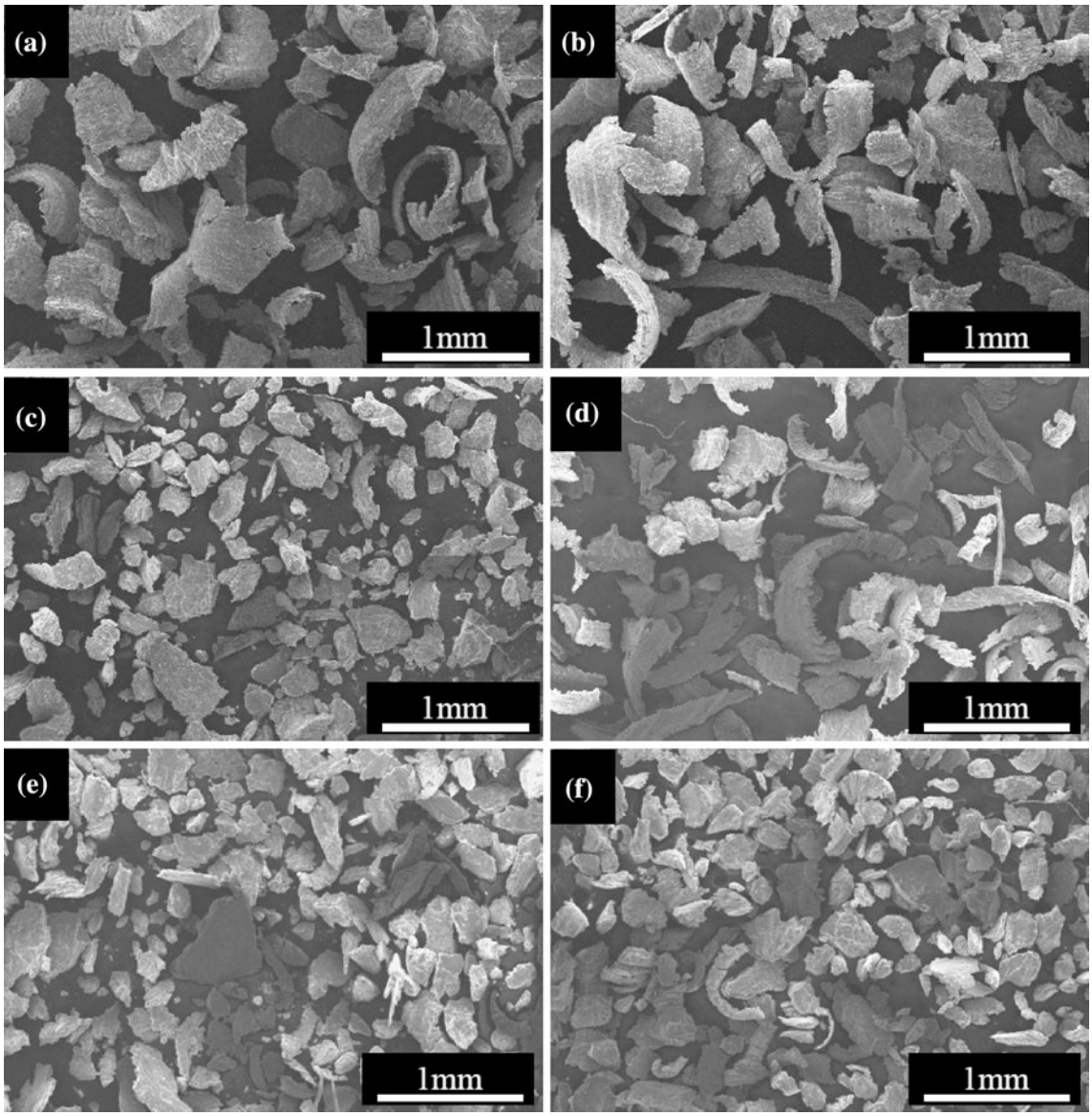

Fig. 9 Wear debris of (a) A359 aluminum, (b) A359 Al/SiC composite, and composite that contains (c) 2 wt.%, (d) 4 wt.%, (e) 6 wt.% and (f)8 wt.% graphite particles under normal load of 0.62 MPa and sliding speed of 0.92 m/s

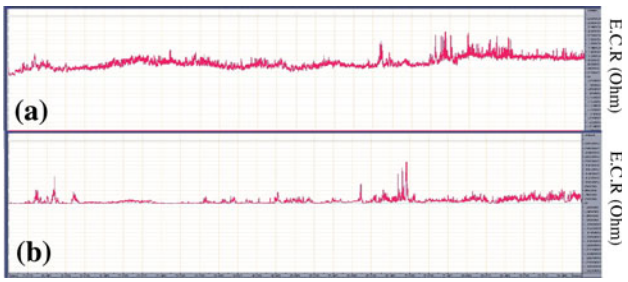

Fig. 10 Electrical contact resistance of (a) A359 aluminum and (b) A359 Al/SiC composite that contains 6 wt.% graphite particles under normal load of 0.62 MPa and sliding speed of 0.73 m/s

4. Conclusion

1. The friction coefficient and wear rate decline as the graphite content increases, but the work surface of the Al/5 wt.% SiC + 8 wt.% Gr.(p) composite exhibits several brittle fractures, which slightly increase the friction coefficient and wear rate. The worn surface of the composite with added 8 wt.% graphite exhibits more fracturing than those with 2-6 wt.%. The friction coefficients of the A359 Al alloy/SiC composites with added graphite are lower than that of the Al/SiC composite.
2. The amount of the film of graphite that is released from the composites on the worn surface increases with the amount of added graphite, and this film of released graphite bonds to the worn surface of the composites and their counterparts.
3. Pieces of wear debris become smaller as more graphite particles are added. However, 8 wt.% graphite particle content yields some large wear debris.
4. The wear rate of the aluminum matrix and the composites was insensitive to the variation in sliding speed and normal loading.

5. The ECR declines as the graphite content increases because the size of the wear debris decreases. However, 8 wt.% graphite content yields higher contact resistance than the 6 wt.% Gr.(p) composite. These results indicate that the wear particles, their size, and their morphology strongly affect the values of ECR: larger debris corresponds to a higher ECR. The electrical contact resistance is insensitive to the variation in sliding speed and normal loading.

Acknowledgments

The authors would like to thank the National Science Council of the Republic of China, Taiwan, for financially supporting this research.

References

1. A.K. Jha, S.V. Prasad, and G.S. Upadhyaya, Sintered 6061 Aluminium Alloy-Solid Lubricant Particle Composites: Sliding Wear and Mechanisms of Lubrication, *Wear*, 1989, **133**, p 163–172
2. P.R. Gibson, A.J. Clegg, and A.A. Das, Wear of Cast Al-Si Alloys Containing Graphite, *Wear*, 1984, **95**, p 193–198
3. G.B. Rudrakshi, V.C. Srivastava, J.P. Pathak, and S.N. Ojha, Spray Forming of Al-Si-Pb Alloys and Their Wear Characteristics, *Mater. Sci. Eng., A*, 2004, **383**, p 30–38
4. G.B. Rudrakshi, V.C. Srivastava, and S.N. Ojha, Microstructural Development in Spray Formed Al-3.5Cu-10Si-20Pb Alloy and its Comparative Wear Behaviour in Different Environmental Conditions, *Mater. Sci. Eng., A*, 2007, **457**, p 100–108
5. V.C. Srivastava, G.B. Rudrakshi, V. Uhlenwinkel, and S.N. Ojha, Wear Characteristics of Spray Formed Al-Alloys and Their Composites, *J. Mater. Sci.*, 2009, **44**, p 2288–2299
6. B.P. Krishnan, M.K. Surappa, and P.K. Rohatgi, The UPAL Process: A Direct Method of Preparing Cast Aluminum Alloy-Graphite Particle Composites, *J. Mater. Sci.*, 1981, **16**, p 1209–1216
7. R.K. Rohatgi and S.V. Prasad, Tribological Properties of Aluminum Alloy Composites, *J. Met.*, 1987, **39**, p 22–26
8. A.A. Baker, Carbon Fibre Reinforced Metals—A Review of the Current Technology, *Mat. Sci. Eng.*, 1975, **17**, p 177–208
9. M. Suwa, K. Komuro, and S. Iijima, Graphite Dispersed Casting Alloys, *Imono*, 1989, **61**, p 139–147
10. Z. Liu, G. Zu, H. Luo, Y. Liu, and G. Yao, Influence of Mg Addition on Graphite Particle Distribution in the Al Alloy Matrix Composites, *J. Mater. Sci. Technol.*, 2010, **26**(3), p 244–250
11. B.C. Pai, G. Ramani, R.M. pillai, and K.G. Satyanarayana, Role of Magnesium in Cast Aluminum Alloy Matrix Composites, *J. Mater. Sci.*, 1995, **30**, p 1903–1911
12. K. Funatani and K. Kurosawa, Composite Coatings Improve Engines, *Adv. Mater. Process.*, 1994, **146**, p 27–29
13. D.G. Evans, P.L. Morris, R.W. Hains, C. Jowett, and P. Achim, *Production Extrusion of AA6061-SiC Metal Matrix Composites*, Alcan, Kingston, 1989
14. A. N. Abd El-Azim, A. M. El-Sheikh, F. A. El-Bassyouni, and S. F. Moustafa, *Proceedings of the 6th International Conference on Mechanical Behavior of Materials*, 1991, Kyoto, Japan, Vol 3, p 441
15. S. Muthukumarasamy, A. Guruprasad, A. Sudhakar, and S. Seshan, Performance of Zinc Alloy Based Metal Matrix Composites Produced Through Squeeze Casting, *Mater. Manuf. Processes*, 1993, **11**, p 351–366
16. G.S. Upadhyaya, Powder Metallurgy, Metal Matrix Composites, an Overview, *Met. Mater. Process.*, 1989, **1**, p 17–28
17. J.-M. Chiou and D.D.L. Chung, Characterization of Metal-Matrix Composites Fabricated by Vacuum Infiltration of a Liquid Metal Under an Inert Gas Pressure, *J. Mater. Sci.*, 1991, **26**, p 2583–2589
18. G.I. Estrada, G.C. Carreno, C.J.L. Cardoso, R.E. Rocha, R.J.M. Herrera, and S.R. Martinez, Effect of Metallic Addition on Mechanical Properties in an Aluminum-Graphite Composite Synthesized by Means of Mechanical Milling, *J. Alloys Compd.*, 2010, **495**(2), p 403–407
19. N. Barekar, S. Tzamtzis, B.K. Dhindaw, J. Patel, N. Hari Babu, and Z. Fan, Processing of Aluminum-Graphite Particulate Metal Matrix Composites by Advanced Shear Technology, *J. Mater. Eng. Perform.*, 2009, **18**(9), p 1230–1240
20. S. Suresha and B.K. Sridhara, Effect of Addition of Graphite Particulates on the Wear Behavior in Aluminum-Silicon Carbide-Graphite Composites, *Mater. Des.*, 2010, **31**(4), p 1804–1812
21. A. Sato and R. Methrabian, Aluminum Matrix Composites: Fabrication and Properties, *Metall. Trans. B*, 1976, **7**, p 443–450
22. C. B. Lin, U.S.A. Invent Patent, No. 5401338, Mar 1995